Active trailer steering control for high-capacity vehicle combinations

Active Trailer Steering Control for High-Capacity Vehicle Combinations

Karel Kural, Pavlos Hatzidimitris, Nathan van de Wouw, Igo Besselink, and Henk Nijmeijer, *Fellow, IEEE*

***Abstract*—In this paper, a new control strategy for the active steering of a trailers of longer and heavier vehicle combinations is proposed to improve both low speed maneuverability and high speed stability. A novelty of the approach is in the use of a single controller structure for all velocities using a gain scheduling method for optimal performance at any velocity. To achieve such a control objective, the problem is initially formulated as a path following problem and subsequently transformed into a tracking problem using a reference model. To support controller design, a generic nonlinear model of a double articulated vehicle, based on a single track model, is employed. The proposed systematic design approach allows to easily adjust the controller for additional trailers or different dimensions, in which only some of the towed vehicles are allowed to steer. The performance of the controller is verified on a high-fidelity multi-body model for evidencing the practical applicability of the approach. Simulation results show substantial reduction of both, the swept path width and tail swing for low speed, and the rearward amplification for high speed.**

***Index Terms*—Active steering, intelligent vehicles, land transportation, vehicle safety and maneuverability.**

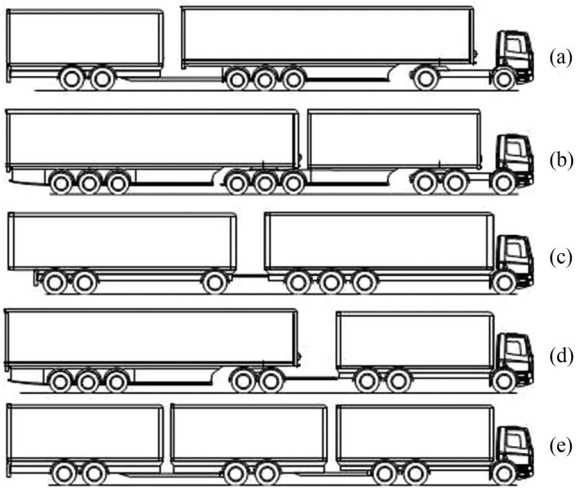

Fig. 1. Examples of HCV configurations.

I. Introduction

ROAD freight transport plays a key role in the European economy. In Europe, about 75% of total inland transport is performed by trucks versus just 18.5% by rail and 6.5% by waterway [1]. Besides that, the quantity of transported goods is continuously increasing, which is related to the development level of national economies. However, this has a substantial impact on the wear and tear of roads as well as on the amount of traffic jams caused by commercial vehicles. Even though OEMs (Original Equipment Manufacturers) are stimulated by the national governments to produce cleaner and more efficient vehicles, e.g., through the EURO 6 standard, road transport still consumes more that 26% of the total energy in Europe [2]. Besides this being an economical argument, it is also an ecological argument: 19% of the greenhouse gases emission is caused by road transport [2].

Although lately fuel prices have decreased significantly, in the future it is expected that prices will eventually start rising again resulting in higher operational costs for transportation companies and fleet owners. Hence, it is clear that reducing the fuel consumption of road transport is desirable from several perspectives. As the intensity of road transport usage is unlikely to diminish in the future, significant improvements in fuel efficiency are needed.

Besides improving the efficiency of combustion engines, a promising alternative are High Capacity Vehicles (HCV).

HCV's are trucks, which typically tow multiple of trailers having also multiple articulation points. An overview of several types of HCV's is given in Fig. 1.

With their increased capacity, originating in length up to 25 meters and weight up to 60 tonnes, HCV's achieve an improved emission efficiency reducing more than 25% of emitted grams Carbon Dioxide/ton/km. [3] compared to the most frequently used conventional combination of tractor with semitrailer. Besides this positive environmental effect, HCV's have also a pos-

Manuscript received April 18, 2017; revised September 23, 2017; accepted October 5, 2017. Date of publication October 27, 2017; date of current version December 18, 2017. *(Corresponding author: Karel Kural.)*

K. Kural is with the Department Mechanical Engineering, Eindhoven University of Technology, Eindhoven 5612 AZ, The Netherlands, and also with HAN Automotive Research, HAN University of Applied Sciences, Arnhem 6826 CC, The Netherlands (e-mail: karel.kural@han.nl).

P. Hatzidimitris was with the Department Mechanical Engineering, Eindhoven University of Technology, Eindhoven, 5612 AZ, The Netherlands. He is now with ASML, Veldhoven 5504 DR, Netherlands (e-mail: p.hatzidimitris@student.tue.nl).

N. van de Wouw is with the Department Mechanical Engineering, Eindhoven University of Technology, Eindhoven 5612 AZ, The Netherlands, with the Department of Civil, Environmental and Geo-Engineering, University of Minnesota, Minneapolis, MN 55455, USA, and also with the Delft Center for Systems and Control, Delft University of Technology, Delft 2628 CD, The Netherlands (e-mail: N.v.d.Wouw@tue.nl).

I. Besselink and H. Nijmeijer are with the Department of Mechanical Engineering, Technische Universiteit Eindhoven, Eindhoven 5612 AZ, The Netherlands (e-mail: i.j.m.besselink@tue.nl; h.nijmeijer@tue.nl).

Color versions of one or more of the figures in this paper are available online at http://ieeexplore.ieee.org.

Digital Object Identifier 10.1109/TIV.2017.2767281

itive economic effect. More cargo transported and a reduced truck/cargo ratio results in less drivers needed to transport same amount of cargo. These positive effects contribute currently to a rising number of HCV's on European roads.

Unfortunately, the length of HCV's also represents a challenge with respect to the low-speed maneuverability and sometimes also high-speed stability, compared to most conventional configurations of commercial vehicles. In this scope, several measures exist to quantify the performance of these vehicles ensuring their safe operation given existing infrastructure [4]. In this paper, the measures we will focus on are the swept path width, and tail swing for low-speed maneuverability. The swept path width is the maximum distance that the rear axle of a vehicle combination tracks inside the path taken by the steering axle in a low speed turn, whereas the tail swing refers to the maximum lateral distance that the outer rearmost point on a vehicle moves outwards, perpendicular to its initial orientation, when the vehicle commences a small-radius turn at low speed. For high-speed stability, which is related to yaw and/or roll instability, a rearward amplification measure is used, being the degree to which the trailing unit(s) amplify or exaggerate lateral acceleration of the hauling unit.

Both low-speed maneuverability and high-speed stability can be significantly improved by active steering of trailers. The actively steered trailer is not a new idea as the first patents [5], [6] were registered already in the early 1930's. Since then, this approach has evolved and was subject of extensive research in the automotive field as well as in robotics. However, the control problem considered in these two fields are essentially different. Namely, in mobile robotics research, the steer angle of the first axle is generally seen as a control input, whereas in automotive field it is the driver who controls the first axle and the control input is associated with the steering of particular trailer axles to satisfy given criteria.

Generally speaking, three different types of controllers exist; firstly, controllers improving only low-speed maneuverability, secondly, controllers only for high-speed instability or, thirdly, combined controllers that can deal with both situations. Each type has its advantages and disadvantages either in performance or implementation demands.

Low-speed controllers are typically associated with the robotic vehicles, employing very often a kinematic model to support the design of the controller [7]–[11]. Although the kinematic model does not include tyre forces, body slip and inertial effects and is substantially simpler than a dynamical one, it provides sufficiently accurate results for the robots that typically drive at low speed. The wheeled robots in these papers also do not have multiple axles per body, which results in significant sideslip of the tyres in case of real HCV's; therewith making kinematic models less suitable for real HCV's even in low-speed. The kinematic models used in the reference above are mostly affine in the control input meaning that classical nonlinear control design methods can be employed.

High-speed controllers are often based on linearized dynamical models by assuming small articulation angles. This is a valid assumption, since in typical operational scenarios, such as a lane change, the articulation angles do not exceed ten degrees. This assumption clearly does not hold for low-speed maneuvering. In [12]–[14], linear quadratic regulator (LQR) methods are used to reduce rearward amplification at high speeds. In [15], a sliding mode controller is proposed based on a simplified three degrees of freedom nonlinear model. Assuming small steering angles and using the lateral tyre forces as a control input, the system becomes affine in the control input. The desired tyre forces that are generated by the controller are then translated into steering angles using an inverse tyre model.

Based on the heading angle method in [16], a new combined controller design is proposed in [17] and [18] for tractor semi-trailer combination. This controller design consists of a feed-forward part based on a kinematic model that operates at low speed only, and PID feedback controller based on a simplified dynamical model, which is applied exclusively at high speeds. The controller aims to reduce the swept path as well as rearward amplification. An alternative combined approach with comparable results, called Virtual Rigid Axle Command Steering (VRACS), is documented in [19]. The controller uses the velocity of articulation angles to steer the towed bodies with the same steer velocity. The steering is delayed with respect to articulation angle velocity and the delays are optimized empirically using simulations.

The contribution of this paper is to solve the combined problem of low-speed maneuverability and high-speed stability of HCV's by proposing a novel and systematic approach on the basis of a sufficiently generic and accurate vehicle model. The uniqueness of the method is based on the employment of a single controller structure for velocities in the range [1–90] km/h using a gain-scheduled feedback and feedforward controller. Optimal performance at any velocity within mentioned range can be achieved for arbitrary vehicle configurations. As a representative case study, we consider a rigid truck, dolly, and semitrailer vehicle combination, as recent research [3] identified this vehicle combination as one of the potential candidates for most efficient means of road transport for years 2020+. The combination, with total length of nearly 28 meters, is capable of carrying 3×782 swap bodies, which are the loading units having high inter-modal potential.

The paper is organized as follows. Section II covers the derivation of a nonlinear dynamical model of double articulated vehicle using the Lagrangian method and the description of the high-fidelity multi-body model that will be used for verification. In Section III, the control problem is formulated and the reference model is derived. In Section IV, a gain-scheduling controller design method is developed based on a linearization of the dynamical model. Controller verification in a number of operational scenarios is documented in Section V. Finally, the discussion and conclusions are presented in Section VI.

II. Vehicle Dynamics Modeling

As described earlier, most of the existing controller designs are based on kinematic models. Although kinematic models are typically much simpler than dynamic models, the former do not take tyre forces into account, and are only valid at low speed and limited tyre slip. Since the goal is to design the controller

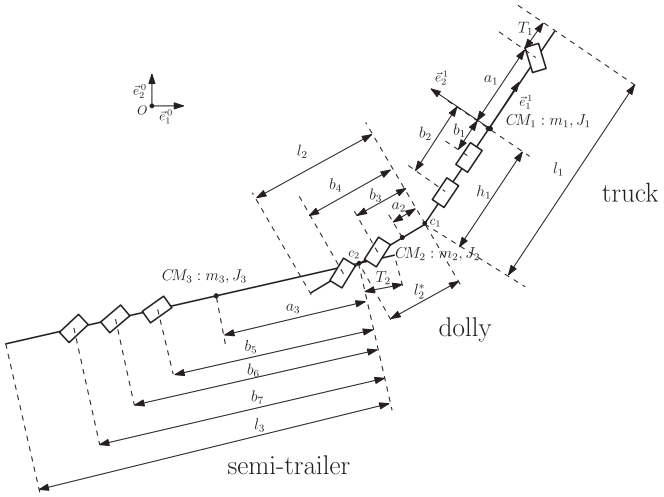

Fig. 2. Double articulated single track model with dimensions and coordinate systems.

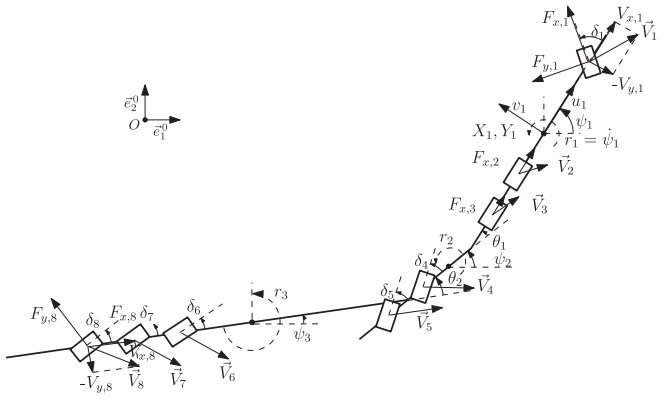

Fig. 3. HCV single track model variables.

structure for active steering that is valid for any realistic speed, a dynamic model that includes also tyre forces is constructed next.

A. State-Space Model

The model is based on a simplified single track (bicycle) model of a double articulated vehicle, see Fig. 2. Each vehicle body (truck, dolly, and semitrailer) is characterized by the dimensions a_i, b_i, l_i, h_i, its mass m_i and moment of inertia J_i. Furthermore, the bodies are assumed to be perfectly rigid and the tyres of each axle were lumped together into single tyre with double stiffness. Horizontal tyre forces are characterized by a linear tyre model, and the cornering stiffness is based on Pacejka's Tyre Magic Formula [20] from available tyre property data. No friction or play is assumed in the articulation joints. The vertical motion is neglected since the model is planar. Therefore, the rotations, which involve movement outwards of x-y plane such as roll and pitch are not considered. The model variables as well as the global, earthfixed, co-ordinate system $\underline{\vec{e}}^0$ are shown in Fig. 3. Note that for clarity reasons only the tyre forces on first and last axle are illustrated, although these act on all axles.

Equations of motion are derived using a Lagrangian approach. Herewith, we employ coordinates defined in the local co-ordinate system $\underline{\vec{e}}^1$ being attached to the truck center of gravity, such as depicted in Fig. 2. The resulting equations will not depend on the orientation ψ_1 of the truck.

Furthermore, note that $\dot{X}_1$ and $\dot{Y}_1$ are the time-derivatives of global position co-ordinates X_1 and Y_1 of the truck center of mass CM_1. θ_1, and θ_2 are the articulation angles between the bodies as defined in Fig. 3. The yaw rate $r_1 = \dot{\psi}_1$ of the truck is defined as time-derivative of the yaw angle ψ_1. Yaw angles of the dolly and semitrailer are defined by means of articulation angles as $\psi_2 = \psi_1 - \theta_1$ and $\psi_3 = \psi_1 - \theta_1 - \theta_2$, respectively. From these yaw angles, the related yaw rates follow: $r_2 = \dot{\psi}_2 = r_1 - \dot{\theta}_1$ and $r_3 = \dot{\psi}_3 = r_1 - \dot{\theta}_1 - \dot{\theta}_2$.

The following set of generalized velocities will be used for the model:

$$\underline{v} = \left[u_1, v_1, r_1, \dot{\theta}_1, \dot{\theta}_2\right]^T \tag{1}$$

where longitudinal velocity u_1 and lateral velocity v_1 in the frame $\underline{\vec{e}}^1$ are given by:

$$\begin{aligned} u_1 &= \dot{X}_1 \cos\psi_1 + \dot{Y}_1 \sin\psi_1, \\ v_1 &= -\dot{X}_1 \sin\psi_1 + \dot{Y}_1 \cos\psi_1. \end{aligned} \tag{2}$$

and can be seen as local quasi coordinates.

A detailed derivation of the equations of motion for the vehicle combination can be found in [21]. The resulting model can be written in the form:

$$M(\theta_1, \theta_2)\dot{\underline{v}} + H(\theta_1, \theta_2, \underline{v}) = \underline{Q_v}. \tag{3}$$

Matrices M, H, and $\underline{Q_v}$ are listed in Appendix A. Next, the equation of motion in (3) are transformed into state-space form, such that the system can be described by a first-order nonlinear differential equation as follows:

$$\dot{x} = f(x) + g(x, u, w(t)), \tag{4}$$

where

$$f(x) = \begin{bmatrix} \dot{\theta}_1 \\ \dot{\theta}_2 \\ -M^{-1}H \end{bmatrix}, \quad g(x, u, w(t)) = \begin{bmatrix} 0 \\ 0 \\ M^{-1}\underline{Q_v} \end{bmatrix}, \tag{5}$$

and $x = \left[\theta_1, \theta_2, \underline{v}^T\right]^T = \left[\theta_1, \theta_2, u_1, v_1, r_1, \dot{\theta}_1, \dot{\theta}_2\right]^T$ are the system states, $u = \left[\delta_4, \delta_5, \delta_6, \delta_7, \delta_8\right]^T$ are the control inputs (dolly and semi-trailer steering angles), see Fig. 3, and $w = \left[\delta_1, F_{x,2}, F_{x,3}\right]^T$ are the external inputs controlled by the driver being the steering angle of the first axle, and traction forces on the driven axles, respectively. The traction forces are employed directly for controlling longitudinal velocity of the truck u_1, without considering longitudinal tyre slip, required to cover true braking situations. This state-space system can be used for simulation purposes and as a basis for the controller design.

B. High-Fidelity Model

Next, the high-fidelity multi-body model will be described that has been validated against experimental test data in [22].

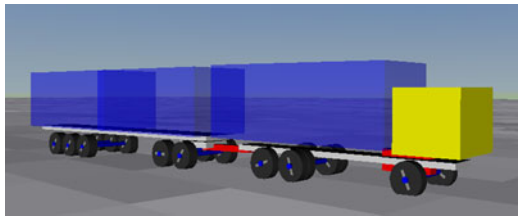

Fig. 4. Multi-body model of rigid truck with dolly and semitrailer created by CVL.

This model will be used for the verification of the controller design, proposed in Section IV, and is primarily intended for the simulation based analysis of performance measures described earlier (such as the swept path width, tail swing and rearward amplification).

The model is built by means the Commercial Vehicle Library (CVL) [23], which is a highly generic library consisting vehicle assemblies (e.g., truck, trailers, semitrailers, etc.) and additional vehicle components (brake system, driveline, etc.) developed in Matlab/SimMechanics by the Eindhoven University of Technology. The purpose of the library is to provide a base for building representative and generic vehicle models while avoiding low-level details (such as, e.g., non-linearities in chassis suspension, roll steer or cabin-chassis suspension) that do not substantially impact overall dynamical behavior. Furthermore, the model can be visualized, using Matlab Virtual Reality Toolbox see Fig. 4.

The chassis of each vehicle is divided in two parts, a frontal and rear segment. They are connected to each other with a rotational degree of freedom enabling to model torsion of the chassis during cornering. Cabin, engine and cargo loading units, which are represented as bodies possessing mass and inertia, are rigidly welded to a neighboring chassis segment hereby not introducing additional degrees of freedom with respect to the chassis. Both axle types, i.e. steerable or driven, are attached to the particular chassis segment by means of rotational and translational degrees of freedom. It enables to model vertical deflection of the suspension, as well as roll and pitch movement of the vehicle body, which is not considered in the state-space model derived in Section II-A. This represents one of the essential differences between the two models contributing to distinctive vehicle behavior especially during highly dynamic maneuvers. Another additional component of the high-fidelity model, which is substantially different to the state space model, is the nonlinear tyre model with relaxation behavior based on the Delft-Tyre library [24]. Since the tyre is the interface between the road and the vehicle responsible for generating reaction forces in all three directions it has dominant impact on the overall vehicle dynamics.

III. Control Problem Formulation

The controller, to be designed in this paper, aims to minimize the swept path width, while ensuring zero tail swing during low-speed maneuvers and aims to suppress rearward amplification during high-speed maneuvers.

To achieve this dual objective, the control problem is initially formulated as a path following problem and subsequently

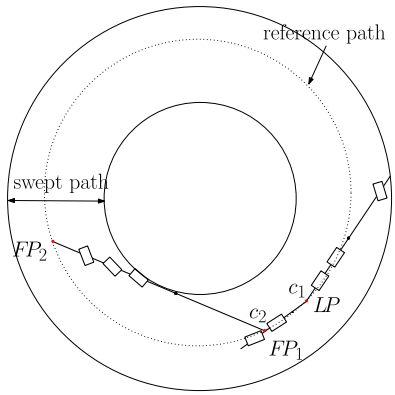

Fig. 5. First combination of LP, FP_1, and FP_2.

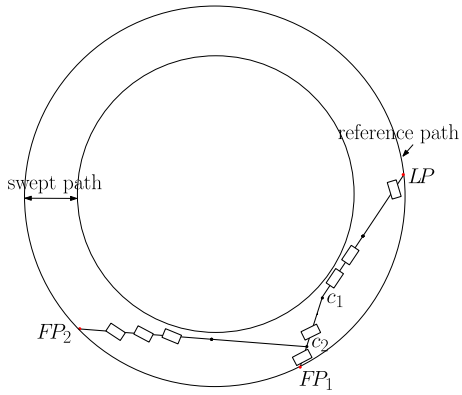

Fig. 6. Second combination of LP, FP_1, and FP_2.

transformed into a tracking problem using a reference model for the dolly and semitrailer. The general idea of the path following strategy is that particular points located on the dolly and semitrailer converge to and follow a path traveled by a particular point on the truck. The follow points on the dolly and semitrailer are referred as FP_1 and FP_2, respectively, whereas the lead point on the truck is referred as LP. Different choices for these points can be made and these choices have distinct advantages and disadvantages. Two combinations of lead and following points are provided in Figs. 5 and 6.

In Fig. 5, the lead point LP is the first coupling point (c_1) and the following points are the second coupling point (c_2) and the rear end of the semitrailer. In Fig. 6, the lead point is at the front of the truck, whereas the follow points are at the rear of both dolly and semitrailer. As can be observed by comparing Figs. 5 and 6, the second combination of lead and follow point not only eliminates the tail swing of the dolly, but also significantly reduces the swept path of the combination. These advantages make the second combination of lead and following points the most favorable choice, which is also advocated in [21].

Remark 1: In case of a high-speed dynamic maneuver, it is proposed to move the lead point closer to the truck center of mass CM_1. The path governed by such selected lead point is generally smoother and thus reference articulation angles (that will be described below) evolve slower. This, in turn, results in smaller lateral accelerations of the dolly and semitrailer, which are more important at high speeds than swept path width. Hence,

all results bellow presented for high-speed maneuver assume the lead point to be at CM_1.

The path following problem can be transformed into a tracking problem using a reference model for the dolly and semitrailer as shown in Fig. 7. In the reference model the location and the orientation of the truck coincides with that of the actual truck and the follow points, which are located on reference path defined by the past evolution of the absolute Cartesian coordinates X_{LP} and Y_{LP} of the lead point, see Figs. 7 and 6. The associated articulation angles of the reference model can then be used as the desired angles for actual vehicle combination. This method is an extension of the concept proposed in [10] and [25] for mobile robots.

In order to find the feasible position for the first follow point (FP_1) that will coincide with the path of the lead point (LP), the distance between the point on the reference path and the first coupling point (X_{C_1}, Y_{C_1}) is calculated. The objective is to find a point on the path for which the distance between that point and the fifth wheel position (X_{C_1}, Y_{C_1}) is equal to the distance l_2, representing the total length of the dolly. To achieve this objective, the time variable $\hat{\tau}_1$ is introduced. This time variable is used to characterize the time instant $(t-\hat{\tau}_1)$ for which the distance between the position of the lead point ($X_{LP}(t-\hat{\tau}_1)$, $Y_{LP}(t-\hat{\tau}_1)$) is feasible for the current position of the first follow point FP_1 (at time t). This time instant is determined by solving the following minimization problem:

$$\hat{\tau}_1(t) := \min_{\tau_1}\{\tau_1 \geq 0 \,|\, f_{\tau_1}(t) = 0\},$$
$$\text{subject to } |\theta_{1\,d}(t)| < \pi/2, \tag{6}$$

where $f_{\tau_1}(t)$ is defined as:

$$f_{\tau_1}(t) := \left(X_{c_1}(t) - X_{LP}(t-\tau_1)\right)^2 + \left(Y_{c_1}(t) - Y_{LP}(t-\tau_1)\right)^2 - {l_2}^2, \tag{7}$$

where $X_{c_1}(t)$ and $Y_{c_1}(t)$ describe the position of the first coupling point at time t, $X_{LP}(t-\tau_1)$ and $Y_{LP}(t-\tau_1)$ describe the position of the front wheel at time $(t-\tau_1)$, and $\theta_{1\,d}(t)$ in (6) is the desired articulation angle between the truck and the dolly and is a result of $\hat{\tau}_1$ (see (9), (10), and (12) below). The position coordinates $X_{c_1}(t)$, $Y_{c_1}(t)$ in (7) can be derived from the lead point position $X_{LP}(t)$ and $Y_{LP}(t)$, which is assumed to be known from the knowledge of yaw rate, longitudinal, and lateral velocity of the truck:

$$X_{c_1}(t) = X_{LP}(t) - l_1\cos(\psi_1(t)),$$
$$Y_{c_1}(t) = Y_{LP}(t) - l_1\sin(\psi_1(t)). \tag{8}$$

Solving the equation $f_{\tau_1} = 0$, in the objective function in (6), may generally result in multiple crossings between the circle with radius l_2 and the lead point path. The minimization part of the problem in (6) describes the search for the minimum value of τ_1, which still satisfies the condition $|\theta_{1\,d}(t)| < \pi/2$, being typically the mechanical limit of the coupling. This condition ensures that solution does not result in the first (i.e., closest to the LP) erroneous minimizer as is shown in Fig. 8, but does result in the correct minimizer, which is the next smallest τ_1 as can be seen in the same figure. In practice, the curvature of the path of the lead point, being defined as inverse to the curve radius, is typically smaller than depicted in Fig. 8, which also avoids the occurrence of the erroneous minimizers.

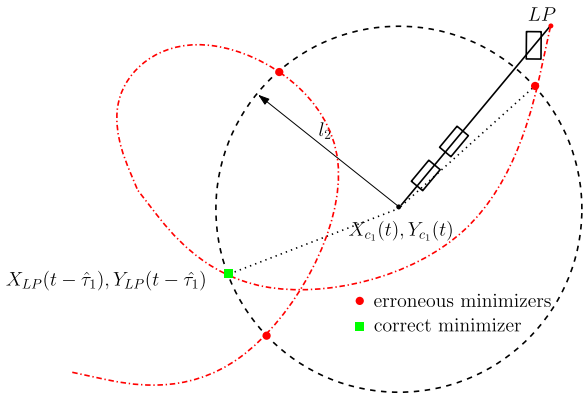

Fig. 8. Minimization process to find $\hat{\tau}_1$.

Then, the desired coordinates of the first follow point can be determined using $\hat{\tau}_1$ from (6):

$$X_{FP_{1\,d}}(t) = X_{LP}(t-\hat{\tau}_1),$$
$$Y_{FP_{1\,d}}(t) = Y_{LP}(t-\hat{\tau}_1). \tag{9}$$

Subsequently, the desired yaw angle of the dolly is derived:

$$\psi_{2\,d}(t) = \text{atan2}(Y_{c_1}(t) - Y_{FP_{1\,d}}(t),\ X_{c_1}(t) - X_{FP_{1\,d}}(t)), \tag{10}$$

where the usage of $atan2$ function ensures an appropriate range of $[-\pi, \pi]$ for $\psi_{2\,d}(t)$. Analogously, the desired position coordinates of the second follow point ($FP_{2\,d}$) can be derived, which in turn leads to a desired yaw angle $\psi_{3\,d}(t)$ for the semitrailer.

Finally, the desired articulation angles are derived from the desired yaw angles as follows:

$$\theta_{1\,d}(t) = ((\psi_1(t) - \psi_{2\,d}(t) + \pi) \mod 2\pi) - \pi, \tag{11}$$
$$\theta_{2\,d}(t) = ((\psi_{2\,d}(t) - \psi_{3\,d}(t) + \pi) \mod 2\pi) - \pi. \tag{12}$$

Remark 2: The modulo operator is needed in (11), since $\psi_1(t)$ is calculated by integration of $r_1(t)$, whereas $\psi_{2\,d}(t)$ follows from an atan2 function. Therefore, $r_1(t)$ does not have a constrained range, while $\psi_{2\,d}(t)$ is constrained to a range $[-\pi, \pi]$. In (12), the modulo operator is needed in the case where $\psi_{2\,d}(t) = \pi - \epsilon$ and $\psi_{3\,d}(t) = -\pi + \varepsilon$, where ϵ and ε are some arbitrary small positive angles. This would result in $\theta_{2\,d}(t) = 2\pi + \epsilon + \varepsilon$, which is reduced to $\theta_{2\,d}(t) = \epsilon + \varepsilon$ by the modulo operator. In both equations, π is added inside the operation and subtracted afterwards, such that $\theta_{1\,d}$ and $\theta_{2\,d}$ are constrained to the interval $[-\pi, \pi]$ instead of the interval $[0, 2\pi]$.

The tracking problem can be stated using the dynamic model (4), (5) derived in Section II-A. The dynamic model, can be now summarized as follows:

$$\dot{x} = f(x) + g(x, u, w(t)),$$
$$y = \begin{bmatrix}\theta_1 \\ \theta_2\end{bmatrix}, \tag{13}$$

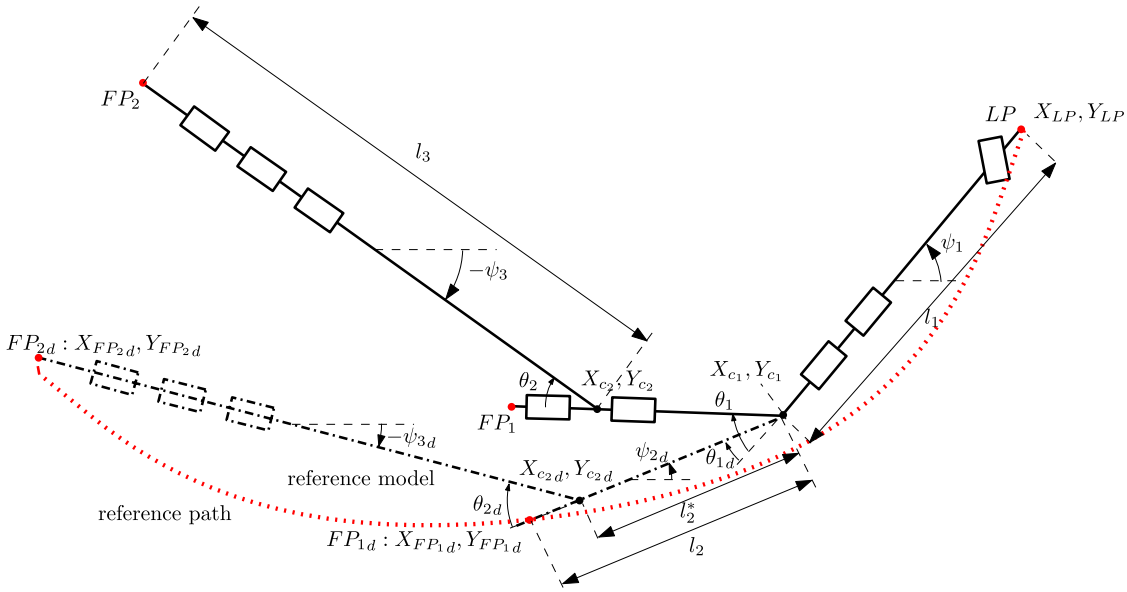

Fig. 7. Reference Model (actual truck, dolly and semitrailer combination in solid, reference configuration in dot dashed line, reference path in red dotted).

where y is the measured output, consisting of the articulation angles. The goal of the control problem is to design a controller for $u = [\delta_4, \delta_5, \delta_6, \delta_7, \delta_8]^T$ such that the output y tracks the reference signal $y_d(t) = \begin{bmatrix} \theta_{1d}(t) \\ \theta_{2d}(t) \end{bmatrix}$; that is:

$$e(t) := y_d(t) - y(t) \to 0, \quad \text{for} \quad t \to \infty, \tag{14}$$

where $\theta_{1d}(t), \theta_{2d}(t)$ are given by (11) and (12). Since the reference signals are based on the reference model, this ensures the accomplishment of the original (path-following) goal of the follow points coinciding with the lead point path. In addition, the closed-loop system should exhibit stable dynamics satisfying the generalized Nyquist criterion.

IV. Controller Design

As mentioned earlier, the control objective is, besides the stable error dynamics, to ensure the convergence of the tracking errors $e_1 = \theta_{1d}(t) - \theta_1(t)$ and $e_2 = \theta_{2d}(t) - \theta_2(t)$ to zero, such that the follow points track the reference path governed by the lead point by means of steering angles on the dolly $[\delta_4, \delta_5]$ and the semitrailer $[\delta_6, \delta_7, \delta_8]$. Using these five steering angles as independent control inputs would result in an over-actuated system, which would result in an unnecessarily complex controller design. Therefore we opt to control the individual dolly axles as well as individual semitrailer axles with equal angles, i.e., $\delta_4 = \delta_5$, and $\delta_6 = \delta_7 = \delta_8$. Furthermore, the controller design combines both feedback and feedforward controllers. Both parts of the controller are being gain scheduled with the longitudinal velocity u_1 as a scheduling variable. This results in the controller structure introduced in Section IV-A. The design of the feedback part of the controller, based on a velocity-dependent linearized vehicle model, is treated in Section IV-B, followed by a closed-loop stability analysis in Section IV-C. Finally, the feedforward design is discussed in Section IV-D.

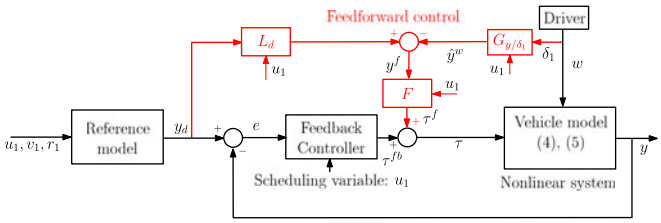

Fig. 9. Controller structure.

A. Controller Structure

In Fig. 9, the proposed controller structure is depicted. It includes the reference model, see Section III, a feedback controller, and a feedforward controller (in red), which together generate the control input $\tau = [\tau_1, \tau_2]^T := [\delta_4, \delta_6]^T$ for the nonlinear system representing the vehicle combination. The input $w = [\delta_1, F_{x,2}, F_{x,3}]^T$ is provided by the driver under the assumption that $F_{x,2} = F_{x,3}$.

The reference model employs information of vehicle states u_1, v_1, and r_1 that are being primarily determined by the driver inputs. In practice, they are either measured or estimated from available measurements in order to derive reference articulation angles $y_d = [\theta_{1d}, \theta_{2d}]^T$. The tracking error $e(t) := y_d(t) - y(t)$ is used as and input to the feedback controller. The gain-scheduled feedback controller incorporates a dynamic decoupler and a multiple input multiple output (MIMO) PID controller. As a scheduling variable the longitudinal velocity u_1 of the first vehicle is being used, which also holds for the feed forward part of the controller. Fig. 9 shows that feedforward controller consist of two branches. The left branch in Fig. 9 includes a low-pass filter L_d, with velocity dependent (u_1) cut-off frequency that prevents high-frequency content of the reference signal in the control loop. The right branch includes a linearized vehicle model G_{y/δ_1}, described in [21], that is using longitudinal velocity as scheduling parameter and denotes the transfer function

from the input of the driver steering angle δ_1 to articulation angles $\hat{y}^w = \left[\hat{\theta}_1^w \ \hat{\theta}_2^w\right]^T$. Subsequently, the difference y^f between the filtered desired articulation angle and the articulation angle introduced by the driver is used as an input for the feedforward controller, which is based on a linearized plant model inversion.

B. Feedback Controller Design

The plant dynamics in (13) is described by a MIMO system with two inputs (τ_1, τ_2) and two outputs (θ_1, θ_2). The intention is to use additional PID controller with e as an input.

The feedback controller design is based on linearized plant models derived from the nonlinear model in (13), that are obtained by linearization around equilibria of steady states characterized by, $\dot{x} = \left[\dot{\theta}_1, \dot{\theta}_2, \dot{u_1}, \dot{v_1}, \dot{r_1}, \ddot{\theta}_1, \ddot{\theta}_2\right]^T = \underline{0}$. Hereto, (3) needs to be solved for $\dot{x} = 0$ resulting in:

$$H(\theta_1, \theta_2, u_1, v_1, r_1) = \underline{Q_v}(\theta_1, \theta_2, u_1, v_1, r_1, \delta_1, \delta_4, \delta_6). \quad (15)$$

Equilibria satisfying (15) are calculated numerically. For this purpose, four variables θ_1, θ_2, u_1, and r_1, were fixed and subsequently the other variables can be obtained by solving (15). These fixed states were chosen because these are most representative to characterize the vehicle combination in terms of the desired nominal steady-state configuration. This yields the equilibrium state x_{eq}, and input vectors τ_{eq} and w_{eq}. Around equilibria, linearized models can be derived, which describe the system behavior close to these points. Since there exist infinitely many equilibria (depending on, e.g., the forward speed or curvature of the path considered), only a relevant subset of equilibria is used as basis for deriving a representative set of linearized models to be used as a basis for controller design.

This subset contains equilibria for driving on a straight path with $u_{1eq} = [1, 90]$ km/h with zero articulation angles, and equilibria for steady-state cornering at $u_1 = 10$ km/h with different curvatures. Using these equilibria, linearized time-invariant systems can be derived of the following form:

$$\begin{aligned} \dot{\hat{x}} &= A(u_1)\hat{x} + B(u_1)\hat{\tau} + B_w(u_1)\hat{w} \\ \hat{y} &= C\hat{x}, \end{aligned} \quad (16)$$

where $\hat{x} = (x - x_{eq})$, $\hat{\tau} = (\tau - \tau_{eq})$, $\hat{w} = (w - w_{eq})$, and system matrices $A(u_1), B(u_1), B_w(u_1)$ are parametrized by the (constant equilibrium) longitudinal velocity u_1. The output matrix C follows from the fact that the two articulation angles compose the measured output:

$$C = \begin{bmatrix} 1 & 0 & 0 & 0 & 0 & 0 & 0 \\ 0 & 1 & 0 & 0 & 0 & 0 & 0 \end{bmatrix}. \quad (17)$$

For the purpose of controller design, we use a transfer function model, corresponding to (16), describing the relation between the inputs τ and w and the outputs y as follows:

$$\hat{y}(s) = G_{y/\tau}(s, u_1)\hat{\tau}(s) + G_{y/w}(s, u_1)\hat{w}(s), s \in \mathbb{C}. \quad (18)$$

These transfer functions are given by:

$$\begin{aligned} G_{y/\tau}(s, u_1) &= C(sI - A(u_1))^{-1}B(u_1) \\ G_{y/w}(s, u_1) &= C(sI - A(u_1))^{-1}B_w(u_1). \end{aligned} \quad (19)$$

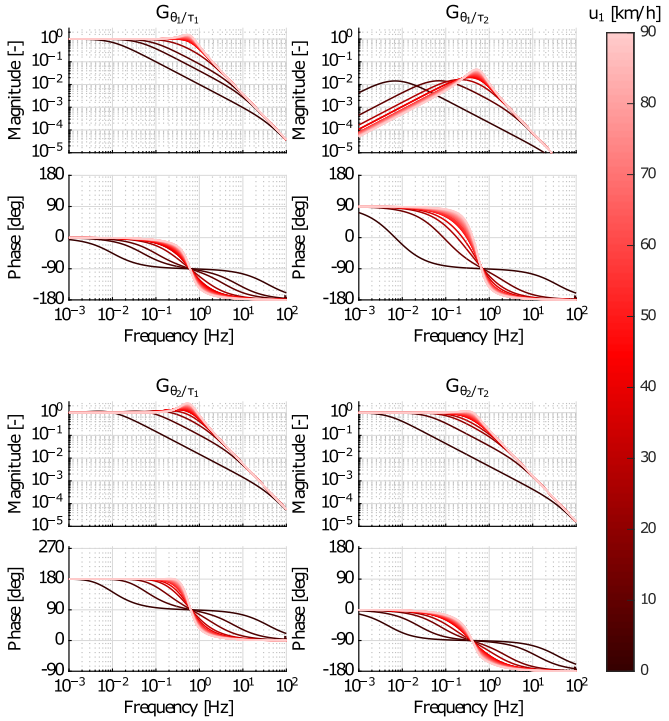

Fig. 10. Bode diagrams of $G_{y/\tau}(j\omega, u_1)$ for straight driving with $u_1^{eq} \in [1, 90]$ km/h and $\theta_1^{eq} = 0, \theta_2^{eq} = 0, r_1^{eq} = 0$.

The linearized models obtained from the straight driving subset will be employed in this work to derive the feed-forward controller and analyze the local stability, whereas the steady-state-cornering based linear models can be used for the cross-verification of the local stability of the feedback controlled system. The transfer function $G_{y/\tau}(s, u_1)$, for straight driving scenarios, can be used to produce Bode plots that give an insight in the dependency of the plant dynamics on the longitudinal velocity u_1 as depicted in Fig. 10. Regarding the Bode plots for steady-state cornering we refer to [21].

In Fig. 10, we care to stress two important aspects. Firstly, the largest differences in dynamic behavior can be seen in the frequency range of 0.4–0.5 Hz, where the system with increasing longitudinal velocity shows decreased damping of the resonance, which in higher velocities eventually evolves in the gain amplification for $G_{\theta_1/\tau_1}(s, u_1)$ and $G_{\theta_2/\tau_1}(s, u_1)$. Secondly, it can be observed that the MIMO system in Fig. 10. is strongly coupled. Namely the influence of τ_1 on θ_2 is substantial and as can be observed in lower left Bode plot of Fig. 10. This coupling has a negative effect on the performance of diagonal feedback controllers, as such coupling can be regarded as an internal disturbance. Hence, dynamical decoupling will be used to partly decouple the input-output dynamics resulting in diagonally dominant dynamics. This is achieved by ensuring that the off-diagonal terms in $G_{y/\tau}(s, u_1)$ are zero by dynamic decoupler design in Fig. 11.

To fully decouple the linearized plant $G_{y/\tau}(s, u_1)$, we define the decoupling matrix $D(s, u_1) = \begin{bmatrix} D_{11} & D_{12} \\ D_{21}(s, u_1) & D_{22} \end{bmatrix}$. In order to maintain the diagonal dynamics, the gains $D_{11} =$

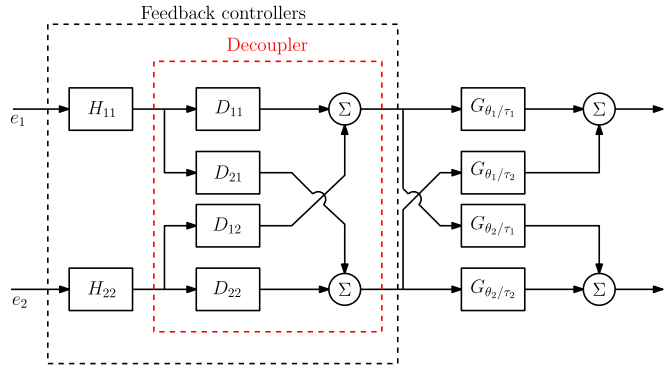

Fig. 11. Feedback controllers with decoupler.

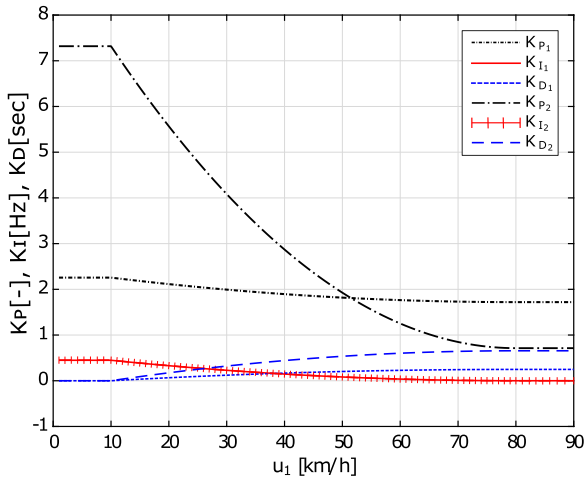

Fig. 12. Gain-scheduling of PID gains. The integral parameters are equal ($K_{I_1} = K_{I_2}$).

$D_{22} = 1$. Since the influence of τ_2 on θ_1 is already insignificant ($G_{\theta_1/\tau_2}(s, u_1)$ is small compared to the other elements in $G_{y/\tau}(s, u_1)$) we take $D_{12} = 0$. Hence, the only remaining gain to design is $D_{21}(s, u_1)$, which is done by solving the equation:

$$G_{\theta_2/\tau_1}(s, u_1)D_{11} + G_{\theta_2/\tau_2}(s, u_1)D_{21}(s, u_1) = 0. \quad (20)$$

This results in $D_{21}(s, u_1) = -G_{\theta_2/\tau_1}(s, u_1)G^{-1}_{\theta_2/\tau_2}(s, u_1)$ (while using D_{11}=1), being the only frequency dependent gain in the decoupling matrix. Furthermore, as both $G_{\theta_2/\tau_1}(s, u_1)$ and $G_{\theta_2/\tau_2}(s, u_1)$ are derived from the plant model that was linearized for particular longitudinal velocity the gain $D_{21}(s, u_1)$ also needs to be scheduled in dependency of truck forward velocity u_1.

The gain scheduling method will be also used to adjust the gains of PID controller $H_{11}(s)$ and $H_{22}(s)$, see Fig. 12, based on gain-scheduling variable u_1. The diagonal PID-type controller is given by $H(s, u_1) = \begin{bmatrix} H_{11}(s, u_1) & 0 \\ 0 & H_{22}(s, u_1) \end{bmatrix}$, where $H_{11}(s, u_1)$ and $H_{22}(s, u_1)$ are two single input single output PID controllers. The input of $H(s, u_1)$ is the column with tracking errors $e = \begin{bmatrix} e_1 & e_2 \end{bmatrix}^T$. The PID-type controllers are defined as follows:

$$H_{11}(s, u_1) = K_{P_1}(u_1) + K_{I_1}(u_1)\frac{1}{s} + \frac{K_{D_1}(u_1)s}{N_1 s + 1},$$
$$H_{22}(s, u_1) = K_{P_2}(u_1) + K_{I_2}(u_1)\frac{1}{s} + \frac{K_{D_2}(u_1)s}{N_2 s + 1}, \quad (21)$$

where $K_{P_1}(u_1)$, $K_{I_1}(u_1)$, $K_{D_1}(u_1)$ are, respectively, the proportional, integral and derivative gains of $H_{11}(s, u_1)$ and $K_{P_2}(u_1)$, $K_{I_2}(u_1)$ and $K_{D_2}(u_1)$ are the corresponding gains of $H_{22}(s, u_1)$. $N_1 = 10\pi$ and $N_2 = 10\pi$ are the first-order low-pass filter constants, which are needed to make the derivative terms proper.

The values correspond to a cut-off frequency of 5 Hz which is appropriate for the governing system dynamics. To ensure a continuous dependency on u_1, the gains will be defined by the quadratic function of longitudinal velocity u_1:

$$K_{P_1}(u_1) = k^0_{P_1} + k^1_{P_1}u_1 + k^2_{P_1}u_1^2,$$
$$K_{I_1}(u_1) = k^0_{I_1} + k^1_{I_1}u_1 + k^2_{I_1}u_1^2,$$
$$K_{D_1}(u_1) = k^0_{D_1} + k^1_{D_1}u_1 + k^2_{D_1}u_1^2,$$
$$K_{P_2}(u_1) = k^0_{P_2} + k^1_{P_2}u_1 + k^2_{P_2}u_1^2,$$
$$K_{I_2}(u_1) = k^0_{I_2} + k^1_{I_2}u_1 + k^2_{I_2}u_1^2,$$
$$K_{D_2}(u_1) = k^0_{D_2} + k^1_{D_2}u_1 + k^2_{D_2}u_1^2. \quad (22)$$

The tuning of the PID controller parameters is based on several low- and high- speed simulations, i.e., for $u_1 = 10$ km/h, and 80 km/h, while aiming to minimize both the tracking errors e and the control inputs τ. As can be seen in Fig. 10, the linearized system is supercritically damped at low speeds ($u_1 < 15$ km/h). This means that at low speeds no overshoot for both articulation angles θ_1, θ_2 based on steering input τ_1, τ_2 occurs, which would eventually result in the increased swept path. Hence the derivative action of a PID controller, that is typically used to provide damping to the closed-loop system, is not needed in this scenario to avoid overshoot. Namely, the proportional and integral constants at $u_1 = 10$ km/h are chosen such that the closed-loop system is still supercritically damped.

At high speeds, where a lane change is considered as a key maneuver, no steady-state cornering takes place. Therefore, no steady-state tracking errors occur; thus, no integral term in the PID controllers is needed to regulate the errors to zero. However, the derivative component of PID controller is essential, as can be seen in Fig. 12, to provide sufficient damping and avoid the rearward amplification, which might eventually result in roll-over accident.

These two assumptions substantially simplify the gain tuning process. Due to the fact that the polynomials are defined by three parameters, three boundary conditions need to be formulated. A requirement is imposed such that $\frac{dK(80)}{du_1} = 0$ for all parameters. Doing this, we force the extremum (minimum for the proportional and integral terms, maximum for the derivative terms) of the polynomial functions to occur at 80 km/h. This forces a monotonic trend of the gains between $u_1 = 10$ and $u_1 = 80$ km/h, since the functions (22) are quadratic ; namely,

such functions show a monotonic trend before (and after) the extremum.

The tuning of the gains has been done manually as follows. At first, the gains were optimized for the single track model and, thereafter, the gains corresponding to each PID controller are scaled, with a factor smaller than 1, based on simulations of the high-fidelity model. The latter step is performed to avoid excessive oscillatory behavior in the control inputs τ of the high fidelity model. This behavior is caused by unmodeled dynamics in single-track model compared to the high-fidelity model, such as the nonlinear tyre dynamics. In Fig. 12, the resulting dependency of the PID gains on the longitudinal velocity u_1 is depicted.

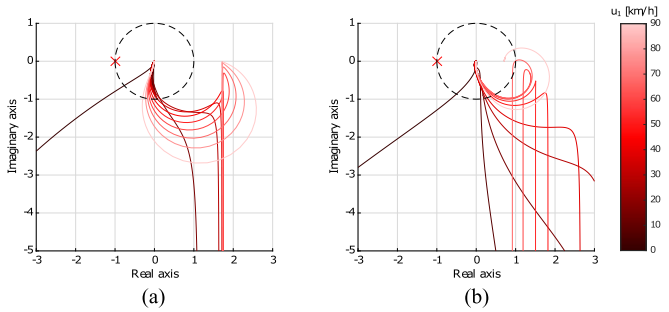

Fig. 13. Nyquist eigenloci of a) $\lambda_1(s)$ and b) $\lambda_2(s)$ corresponding to the open-loop systems $G_{OL,11}(s,u_1)$ and $G_{OL,22}(s,u_1)$, respectively, for to gain-scheduled controllers of the dolly (left), and the semitrailer (right).

C. Closed-Loop Stability Analysis

The tuning of feedback controllers should result in stable closed-loop system with sufficient stability margin for all linearized plants ($u_1 \in [1, 90]$ km/h).

To investigate the closed-loop stability of the MIMO system, depicted in Fig. 11, the generalized Nyquist stability criterion [26] is used. The MIMO closed-loop transfer function matrix is given by $G_{CL}(s,u_1) = G_{OL}(s,u_1)\left(I + G_{OL}(s,u_1)\right)^{-1}$, where $G_{OL}(s,u_1) = G_{y/\tau}(s,u_1)D(s,u_1)H(s,u_1)$ is the open-loop transfer function matrix, which is combining the previously defined linearized plants, the decoupler, and the controller, respectively.

The generalized Nyquist criterion states that the number of unstable closed-loop poles equals the (net) number of times the locus of $\det(I + G_{OL}(s,u_1))$ encircles the origin in clockwise direction plus the number of unstable open-loop poles. Using the state-space linearized plant models in (16), it has been verified within the scope of [21] that number of open-loop unstable poles is zero. Therefore, to obtain a stable closed-loop system no encirclements of the origin in clockwise direction should occur in the Nyquist plot of $\det(I + G_{OL}(s,u_1))$.

The disadvantage of using a locus of the determinant is that the resulting Nyquist plot combines the effects of the controllers $H_{11}(s,u_1)$ and $H_{22}(s,u_1)$ into one graph. This is not desirable, as the controllers can not be tuned independently in this way. Hence, instead of the determinant locus we will use the eigenvalue loci of $G_{OL}(s,u_1)$.

In order to do that, we rewrite $\det(I + G_{OL}(s,u_1))$ as a function of $\lambda_i(s)$, which are the eigenvalues of $G_{OL}(s,u_1)$ that are parametrized by s:

$$\det(I + G_{OL}(s,u_1)) = \prod_{i=1}^{2}(1 + \lambda_i(s)). \tag{23}$$

It should be emphasized that eigenvalues $\lambda_1(s)$ and $\lambda_2(s)$ do not refer to the poles of the system, but to the eigenvalues of the open-loop transfer function matrix $G_{OL}(s,u_1)$ (for $s = j\omega$) that has size of 2×2.

Because, for $s = j\omega$,

$$\arg\langle\det(I + G_{OL}(j\omega))\rangle = \sum_{i=1}^{2}\arg\langle 1 + \lambda_i(j\omega)\rangle, \tag{24}$$

we have that, any change in the angle of $\det(I + G_{OL}(s,u_1))$ results from the sum of phase changes in the terms $(1 + \lambda_i(s))$ (for $i = 1, 2$). Hence, encirclement of the origin in the complex plane by $\det(I + G_{OL}(s,u_1))$ can be computed from the encirclements of $(-1, 0j)$ by the combination of the eigenloci of $\lambda_1(s)$ and $\lambda_2(s)$ [27].

As shown in Fig. 10, the gain of $G_{\theta_1/\tau_2}(s,u_1) \approx 0$. Considering this fact, and the effect of gain-scheduled dynamical decoupler, the linearized open loop transfer function matrix $G_{OL}(s,u_1)$ can be considered as diagonal, i.e. $G_{OL,12}(s) \approx G_{OL,21}(s) \approx 0$. Thus, the eigenvalues of $G_{OL}(s,u_1)$ are the systems in the diagonal, i.e. $\lambda_1(s) \approx G_{OL,11}(s,u_1)$, and $\lambda_2(s) \approx G_{OL,22}(s,u_1)$. This is equivalent to considering the diagonal system as a multiple Single Input Single Output (SISO) system and assessing the stability of the two systems $G_{OL,11}(s,u_1)$, and $G_{OL,22}(s,u_1)$ using normal Nyquist criterion. This enables separate tuning of the controllers $H_{11}(s,u_1)$ and $H_{22}(s,u_1)$ for robust stability. Nyquist plots of $\lambda_1(s)$ and $\lambda_2(s)$ for straight driving and $r_1^{eq}, \theta_1^{eq}, \theta_2^{eq} = 0$ are shown in Fig. 13, where it is made clear that stability margins of all closed-loop systems (i.e., for $u_1 \in [1, 90]$ km/h) are sufficiently large. Given the asymptotic stability of the linearized dynamics (through satisfaction of the generalized Nyquist criterion), we can now conclude that the equilibria (used as a basis for linearization) are locally asymptotically stable equilibria of the nonlinear plant dynamics in (13) in closed loop with the proposed controller.

D. Feedforward Design

Besides the feedback controller, also the feedforward controller is gain-scheduled on the basis of u_1. In particular, the coefficients of the transfer functions corresponding to a 2×2 feedforward controller are being scheduled with u_1. For the controller $F(s)$, shown in Fig. 9, the plant inversion method was applied in a sense described in [26]. In order to make the controller causal a second-order Butterworth low-pass filter $L(s)$ was included. The order of the filter was chosen such that $F(s)$ is proper, whereas the choice of cut-off frequency of 50 Hz aimed to primarily remove high-frequency content from the reference signals. Therefore $F(s) = G_{y/\tau}(s)^{-1}L(s)$.

Because the reference signal y_d may also contain high-frequency noise (e.g. due to a sampled data implementation

that is needed for practical applications), an extra 4th-order Butterworth low-pass filter $L_d(s)$ is added, see Fig. 9, with a u_1-dependent cut-off frequency.

The last component of the feedforward controller design involves extra path that takes care of the effect of the driver input on the output represented by articulation angles via transfer function $G_{y/\delta_1}(s)$, see Fig. 9. From a control point of view, the input from the driver can be considered as a disturbance. Physically, this means that when the driver steers, the vehicle starts to corner, which induces articulation between the bodies. The effect of this exogenous driver input is relatively large, and if not taken into account, a feedforward controller based on y_d only may actually degrade instead of improve the performance of the system. Hence $\hat{y}^w = G_{y/\delta_1}(s)$ is subtracted from the (filtered) reference signal y_d. The resulting signal $y^f = y_d - \hat{y}^w$ is the input of the feedforward controller $F(s)$. The interpretation of y^f can be seen as the difference between the desired articulation angles and the articulation angles that would be induced only by driver action δ_1. If the feedforward controller would be an exact representation of the (nonlinear) plant, then the tracking error would converge to zero. In practice, this means that the feedforward is only exact for small perturbations when the vehicle is driving straight (since we only use u_1 as scheduling variable). However, the resulting errors are still small for large articulation angles, which the feedback controller can regulate the errors towards zero, as is shown in next section.

V. Controller Simulations

In this section, a number of simulation studies are presented in order to verify the functionality of the controller that is based on the nonlinear single track model. The aim is to benchmark the controller performance for both high- and low-speed scenarios compared to the baseline uncontrolled vehicle combination. As an objective assessment measure, the metrics such as defined by the PBS framework [4] will be used. Namely, the rearward amplification will be used for high-speed performance assessment and the vehicle swept path width for low-speed maneuverability. For these simulation studies, the high fidelity multi-body model described in Section II-B will be used in order to also assess the robustness of proposed control strategy in the presence of dynamics aspects ignored in the single track model used for controller synthesis.

A. Low-Speed Maneuvering

The low-speed maneuverability is tested for a roundabout maneuver (with a radius of 12.5 m) with constant longitudinal velocity u_1=10 km/h. The maneuver consists of the entry into the roundabout, followed with the approximately one and half turn and finished by exiting the roundabout. The resulting swept path for both the uncontrolled and controlled vehicle combination is shown on Fig. 14 as well as the path of lead and follow points. The swept path is defined by the outer path of the front right corner of the truck and the path of the left side of the semitrailer. The decisive performance factor is the swept path width, which is for the uncontrolled case 11.2 m (current EU legislation allows only for 7.2 m), whereas with the proposed path-following

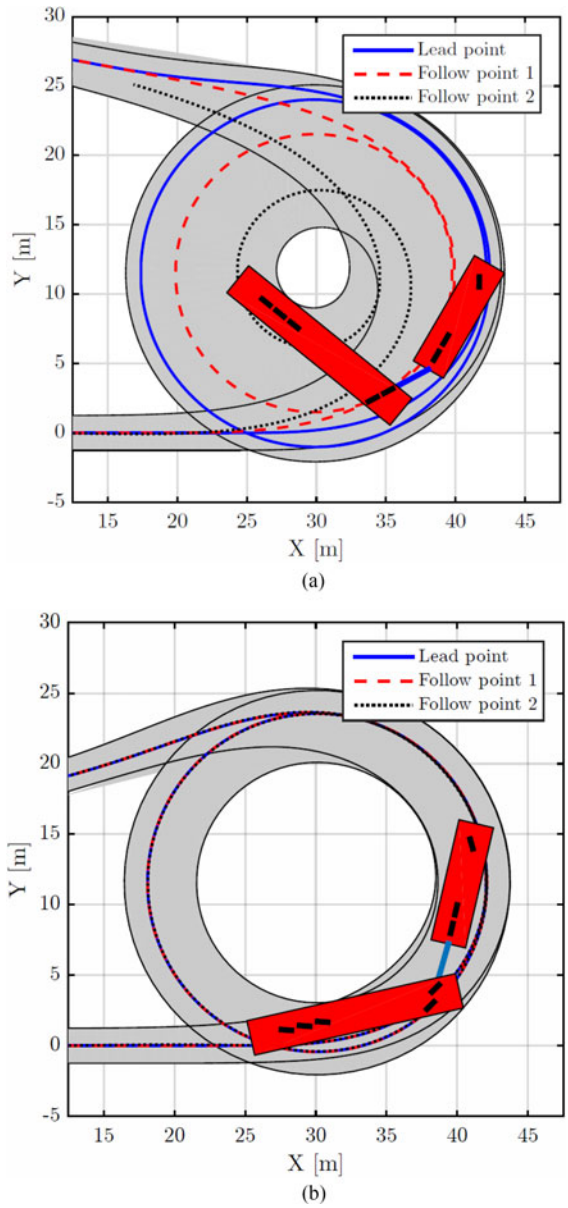

Fig. 14. Vehicle swept path during low-speed maneuvering. (a) Noncontrolled Situation. (b) Path Following Control.

controller it can be reduced to 5.1 m, representing an improvement of approximately 55%. The driver and control inputs are shown in Fig. 15(a). As can be seen, the feedforward part of the controller, τ_i^f, provides main contributions to the steering signals. Hence, it can be deduced that feedforward controller performs well even for large articulation and steering angles, although it is based on a linearization around straight path driving. The imperfections of the feedforward are mostly corrected by feedback controller, τ_i^{fb}, which is leads to close tracking of the reference articulation angles such as depicted in Fig. 15(b) and (c).

B. High-Speed Stability

For the high-speed stability assessment, we perform a lane change maneuver at 80 km/h, where the yaw and roll stability

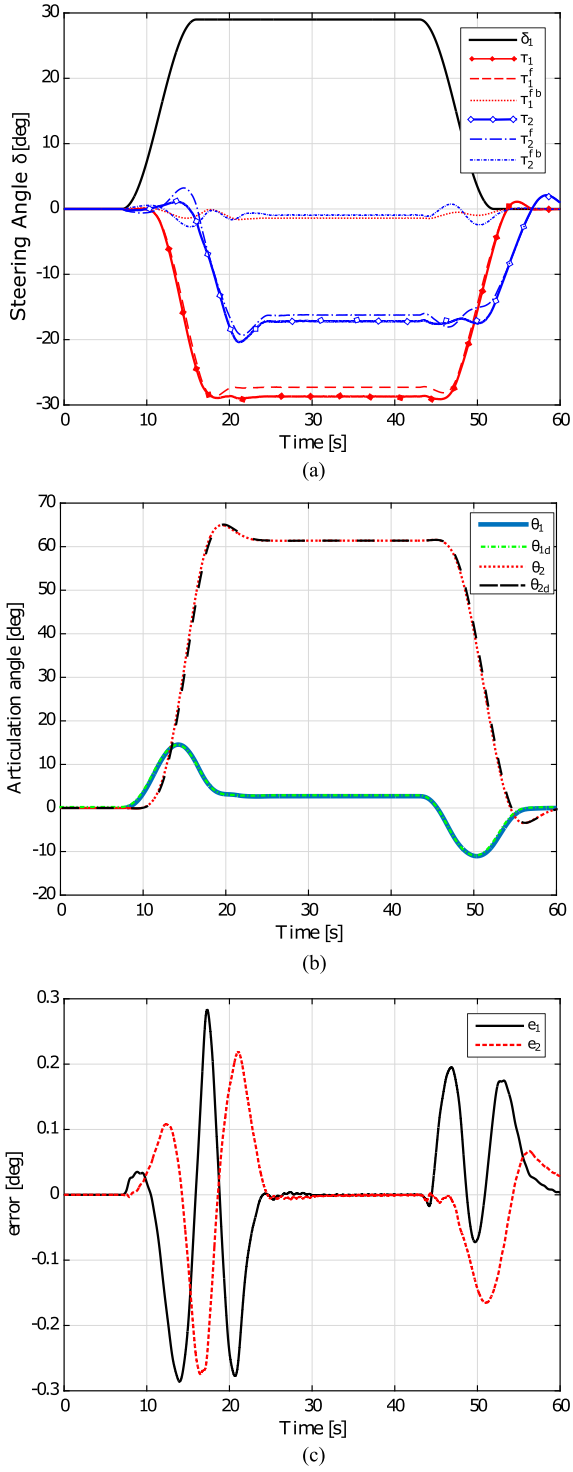

Fig. 15. Low-speed maneuvering performance. (a) Driver and controller inputs. (b) Reference and actual articulation angles. (c) Tracking errors $e_1 = \theta_{1\,d} - \theta_1$ and $e_2 = \theta_{2\,d} - \theta_2$.

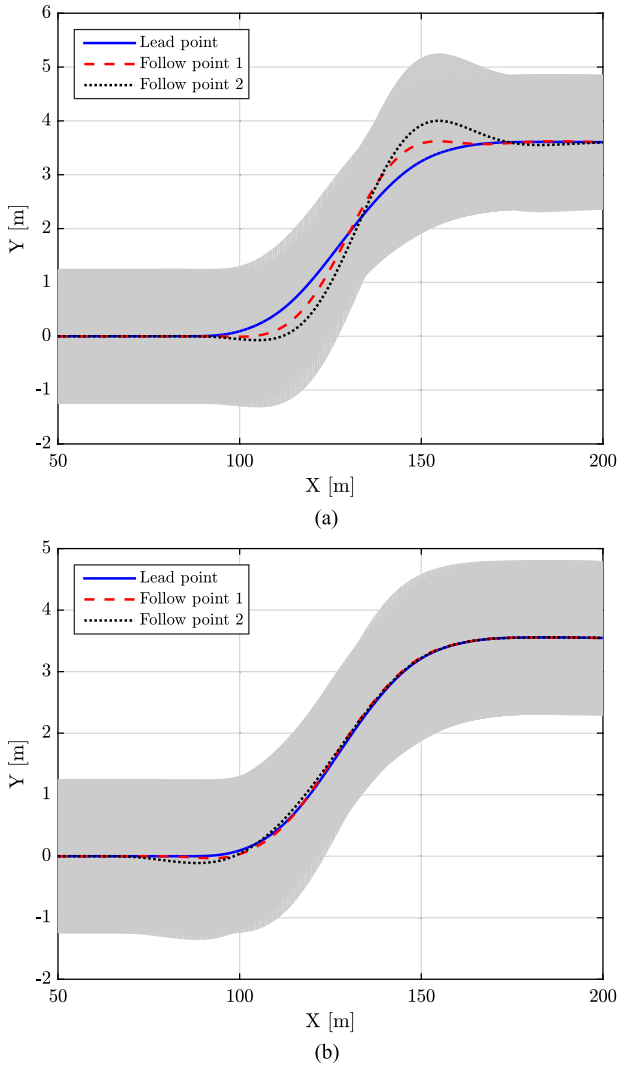

Fig. 16. Vehicle swept path during high speed maneuver. (a) Noncontrolled Situation. (b) Path Following Control.

can become an issue for HCV. The maneuver is performed using a predefined profile of the steering angle δ_1; that is single period sinusoid with frequency of 0.4 Hz. The frequency is chosen according to [4] due to its maximal gain for commercial vehicles handling response resulting typically in higher rearward amplification, that will be used as assessment criterion. The rearward amplification describes the ratio of the maximal achieved lateral acceleration of the dolly (RA_{21}) and the semitrailer (RA_{31}) compared to the maximal achieved lateral acceleration of the truck; namely, on the second and third axle of the dolly and semitrailer, respectively, and the first axle of the truck.

A benchmark comparison of the lane change scenario for controlled and noncontrolled case is again provided. The path comparison is shown in Fig. 16, followed by lateral acceleration a_{yi} for all vehicles in the combination in Fig. 17. For the noncontrolled case, both dolly and semitrailer paths exhibit lateral acceleration overshoot compared to the lead path of the truck. This is projected to the vehicle swept path that is designated by the gray region in Fig. 16(a). Furthermore, one can observe lateral acceleration amplification along the vehicle combination resulting in rather high values of $RA_{21} = 1.68$ and $RA_{31} = 2.05$. When the path following controller is engaged, the path of the dolly and semitrailer is much smoother and without overshoots. The amplification of the lateral acceleration is suppressed resulting in $RA_{21} = 1.12$ and $RA_{31} = 0.81$, representing a reduction

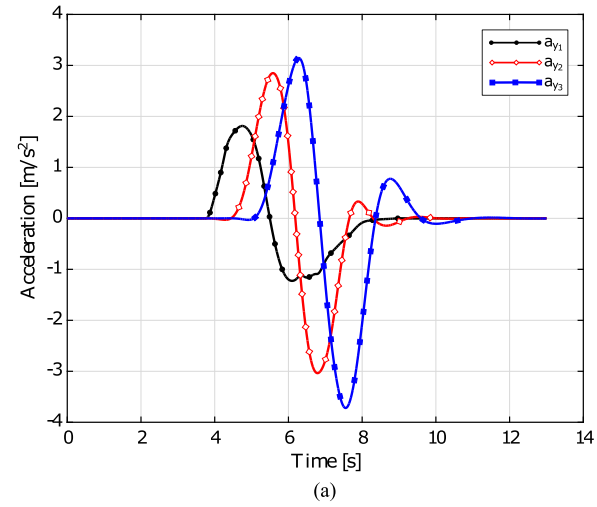

(a)

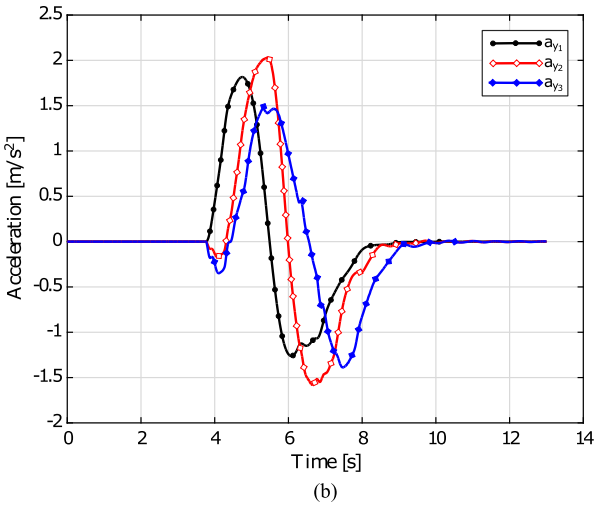

(b)

Fig. 17. Lateral accelerations of the vehicles during high speed maneuver. (a) Noncontrolled Situation. (b) Path Following Control.

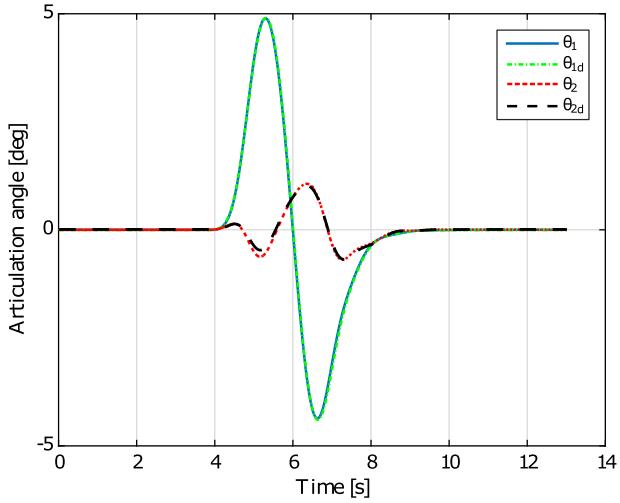

Fig. 18. Reference and actual articulation angles.

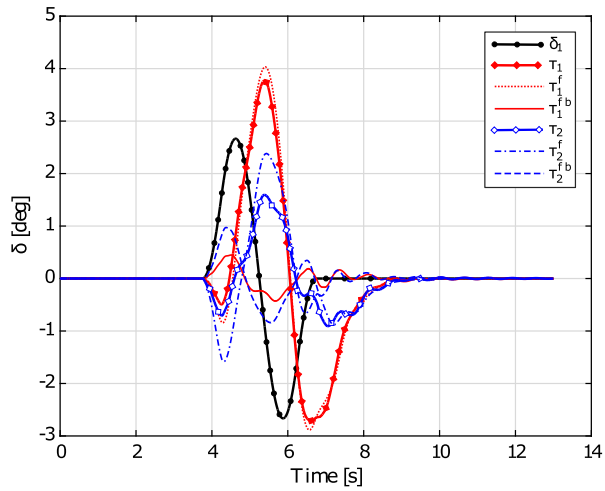

Fig. 19. Driver and controller inputs.

of 30% and 60%, respectively, and it physically means that the lateral acceleration of all vehicles in the combination is quite uniform, which generally reduces the risk of rollover accident.

Although the path following control substantially improves the performance of the vehicle combination, one can observe that the control is slightly suboptimal particularly in the beginning of the maneuver due to feed forward contributions depicted on Fig. 19. Namely, the dolly and semi-trailer axles start to steer in the opposite direction of δ_1. This causes an additional tail-swing and small tracking errors in transients as can be seen in Figs. 16(b) and 18, respectively. This problem is caused by the difference between the high fidelity multi-body model and the single-track model. Since the feedforward controller is based on the single-track model, it is not exact for the multi-body model. This becomes in particular apparent at high-speeds, where unmodeled dynamics in the single-track model, such as for example roll motion, affects the vehicle combination behavior. This effect van be explained in more detail as follows. The reference model uses the actual states (u_1, v_1, r_1) to derive the reference signals y_d, which are then subtracted from $\hat{y}^w$ (see Fig. 9). The $\hat{y}^w$ signals follow from the linearized plant $G_{y/\delta_1}(s)$, which is based on the linearized single-track model. Thus, the resulting signal y^f, which is the input for the feedforward filter $F(s)$, is inexact for the high-fidelity model. A possible solution is to use the single-track model as a state predictor to provide estimated states (u_1, v_1, r_1) as an input to the reference model, see [21].

Summarizing, these results show that

1) the proposed controller can provide significant improvement in both low- and high-speed performance of the commercial vehicle combinations,
2) the uniform controller structure can be used for both type of maneuvers,
3) the controller design is robust against unmodeled dynamics.

VI. Conclusion

In this paper, a generic active trailer steering strategy is developed and applied to truck-dolly-semitrailer combination. The proposed path-following based control method uses gain-scheduling approach to ensure high performance at both low- and high-speeds. The controller improves both the maneuverability at low speeds and improves lateral stability at high speeds. The swept path width and rearward amplification are considered

as assessment criteria for the performance of the vehicle combination. The benefits of the proposed control approach are as follows. Firstly, the method uses single controller structure that can be robustly applied for any velocity in range of 1–90 km/h. Secondly, the usage of the controller leads to significant improvement of the performance, namely at low speed the reduction of swept path reaches 55% and rearward amplification at the high speed is decreased by 33% and 60%, for first and second towed vehicle, respectively. The effectiveness of proposed steer strategy has been tested by extensive simulations with a high-fidelity experimentally validated model, indicating the robustness of the design.

APPENDIX A
VEHICLE MODEL MATRICES

The entries $M_{ij}, i, j \in \{1, 2, ..., 5\}$, of the mass matrix M are given by

$$
\begin{aligned}
M_{1,1} &= m_1 + m_2 + m_3 \\
M_{1,2} &= M_{2,1} = 0 \\
M_{1,3} &= M_{3,1} = -m_3 \left(a_3 \sin(\theta_1 + \theta_2) + l_2^* \sin(\theta_1)\right) \\
&\quad - a_2 m_2 \sin(\theta_1) \\
M_{1,4} &= M_{4,1} = m_3 \left(a_3 \sin(\theta_1 + \theta_2) + l_2^* \sin(\theta_1)\right) \\
&\quad + a_2 m_2 \sin(\theta_1) \\
M_{1,5} &= M_{5,1} = a_3 m_3 \sin(\theta_1 + \theta_2) \\
M_{2,2} &= m_1 + m_2 + m_3 \\
M_{2,3} &= M_{3,2} = -m_3 \left(h_1 + a_3 \cos(\theta_1 + \theta_2) + l_2^* \cos(\theta_1)\right) \\
&\quad - m_2 \left(h_1 + a_2 \cos(\theta_1)\right) \\
M_{2,4} &= M_{4,2} = m_3 \left(a_3 \cos(\theta_1 + \theta_2) + l_2^* \cos(\theta_1)\right) \\
&\quad + a_2 m_2 \cos(\theta_1) \\
M_{2,5} &= M_{5,2} = a_3 m_3 \cos(\theta_1 + \theta_2) \\
M_{3,3} &= ({a_2}^2 + {h_1}^2) m_2 + ({a_3}^2 + {h_1}^2 + {l_2^*}^2) m_3 + J_1 \\
&\quad + 2 a_3 h_1 m_3 \cos(\theta_1 + \theta_2) + 2 a_2 h_1 m_2 \cos(\theta_1) + J_2 \\
&\quad + 2 a_3 l_2^* m_3 \cos(\theta_2) + 2 h_1 l_2^* m_3 \cos(\theta_1) + J_3 \\
M_{3,4} &= M_{4,3} = -J_2 - J_3 - m_2 {a_2}^2 - h_1 m_2 \cos(\theta_1)\, a_2 \\
&\quad - 2 m_3 \cos(\theta_2)\, a_3 l_2^* - h_1 m_3 \cos(\theta_1 + \theta_2)\, a_3 \\
&\quad - h_1 m_3 \cos(\theta_1)\, l_2^* - m_3 ({a_3}^2 + {l_2^*}^2) \\
M_{3,5} &= M_{5,3} = -J_3 - {a_3}^2 m_3 - a_3 h_1 m_3 \cos(\theta_1 + \theta_2) \\
&\quad - a_3 l_2^* m_3 \cos(\theta_2) \\
M_{4,4} &= J_2 + J_3 + m_2 {a_2}^2 + m_3 ({a_3}^2 + {l_2^*}^2) \\
&\quad + 2 m_3 \cos(\theta_2)\, a_3 l_2^* \\
M_{4,5} &= M_{5,4} = m_3 {a_3}^2 + l_2^* m_3 \cos(\theta_2)\, a_3 + J_3 \\
M_{5,5} &= J_3 + m_3 {a_3}^2.
\end{aligned}
$$

The entries $H_i, i \in \{1, 2, ..., 5\}$, of the column H read

$$
\begin{aligned}
H_1 &= m_1 (-r_1 v_1) + m_2 \left(h_1 r_1^2 - r_1 v_1 + a_2 r_1^2 \cos(\theta_1)\right) \\
&\quad + m_2 \left(a_2 \dot{\theta_1}^2 \cos(\theta_1) - r_1 v_1 - 2 a_2 r_1 \dot{\theta_1} \cos(\theta_1)\right) \\
&\quad + m_3 \left(h_1 r_1^2 + a_3 r_1^2 \cos(\theta_1 + \theta_2) + l_2^* \dot{\theta_1}^2 \cos(\theta_1)\right) \\
&\quad + m_3 \left(+ a_3 \dot{\theta_2}^2 \cos(\theta_1 + \theta_2) + l_2^* r_1^2 \cos(\theta_1)\right) \\
&\quad + m_3 \left(2 a_3 r_1 \dot{\theta_1} \cos(\theta_1 + \theta_2) - 2 a_3 r_1 \dot{\theta_2} \cos(\theta_1 + \theta_2)\right) \\
&\quad + m_3 \left(-2 a_3 \dot{\theta_1} \dot{\theta_2} \cos(\theta_1 + \theta_2) - 2 l_2^* r_1 \dot{\theta_1} \cos(\theta_1)\right) \\
&\quad + m_3 \left(a_3 \dot{\theta_1}^2 \cos(\theta_1 + \theta_2) + l_2^* \dot{\theta_1}^2 \cos(\theta_1)\right), \\
H_2 &= m_2 \left(-a_2 \sin(\theta_1)\, {r_1}^2 + 2 a_2 \sin(\theta_1)\, r_1 \dot{\theta_1} + u_1 r_1\right) \\
&\quad - m_2 a_2 \sin(\theta_1)\, \dot{\theta_1}^2 + m_3 \left(r_1 u_1 - a_3 {r_1}^2 \sin(\theta_1 + \theta_2)\right) \\
&\quad + m_3 \left(-a_3 \dot{\theta_1}^2 \sin(\theta_1 + \theta_2) - a_3 \dot{\theta_2}^2 \sin(\theta_1 + \theta_2)\right) \\
&\quad + m_3 \left(-l_2^* {r_1}^2 \sin(\theta_1) + 2 a_3 r_1 \dot{\theta_1} \sin(\theta_1 + \theta_2)\right) \\
&\quad + m_3 \left(2 a_3 r_1 \dot{\theta_2} \sin(\theta_1 + \theta_2) - 2 a_3 \dot{\theta_1} \dot{\theta_2} \sin(\theta_1 + \theta_2)\right) \\
&\quad + m_3 \left(2 l_2^* r_1 \dot{\theta_1} \sin(\theta_1) - l_2^* \dot{\theta_1}^2 \sin(\theta_1)\right) + m_1 r_1 u_1, \\
H_3 &= m_2 \left(a_2 h_1 \sin(\theta_1)\, \dot{\theta_1}^2 - 2 a_2 h_1 r_1 \sin(\theta_1)\, \dot{\theta_1}\right) \\
&\quad + m_2 \left(-h_1 r_1 u_1 - a_2 r_1 u_1 \cos(\theta_1) + a_2 r_1 v_1 \sin(\theta_1)\right) \\
&\quad + m_3 \left(a_3 r_1 v_1 \sin(\theta_1 + \theta_2) - a_3 r_1 u_1 \cos(\theta_1 + \theta_2)\right) \\
&\quad + m_3 \left(-l_2^* r_1 u_1 \cos(\theta_1) + l_2^* r_1 v_1 \sin(\theta_1) - h_1 r_1 u_1\right) \\
&\quad + m_3 \left(a_3 h_1 \dot{\theta_2}^2 \sin(\theta_1 + \theta_2) + a_3 l_2^* \dot{\theta_2}^2 \sin(\theta_2)\right) \\
&\quad + m_3 \left(h_1 l_2^* \dot{\theta_1}^2 \sin(\theta_1) - 2 h_1 l_2^* r_1 \dot{\theta_1} \sin(\theta_1)\right) \\
&\quad + m_3 \left(-2 a_3 h_1 r_1 \sin(\theta_1 + \theta_2) \left(\dot{\theta_1} + \dot{\theta_2}\right)\right) \\
&\quad + m_3 \left(2 a_3 h_1 \dot{\theta_1} \dot{\theta_2} \sin(\theta_1 + \theta_2) - 2 a_3 l_2^* r_1 \dot{\theta_2} \sin(\theta_2)\right) \\
&\quad + m_3 \left(2 a_3 l_2^* \dot{\theta_1} \dot{\theta_2} \sin(\theta_2) + a_3 h_1 \dot{\theta_1}^2 \sin(\theta_1 + \theta_2)\right), \\
H_4 &= m_2 \left(a_2 h_1 {r_1}^2 \sin(\theta_1) - a_2 r_1 v_1 \sin(\theta_1)\right) \\
&\quad + m_3 \left(a_3 r_1 u_1 \cos(\theta_1 + \theta_2) - a_3 r_1 v_1 \sin(\theta_1 + \theta_2)\right) \\
&\quad + m_3 \left(a_3 h_1 {r_1}^2 \sin(\theta_1 + \theta_2) - a_3 l_2^* \dot{\theta_2}^2 \sin(\theta_2)\right) \\
&\quad + m_3 \left(+ h_1 l_2^* {r_1}^2 \sin(\theta_1) + 2 a_3 l_2^* r_1 \dot{\theta_2} \sin(\theta_2)\right) \\
&\quad + m_3 \left(-l_2^* r_1 v_1 \sin(\theta_1) + l_2^* r_1 u_1 \cos(\theta_1)\right) \\
&\quad - m_3 2 a_3 l_2^* \dot{\theta_1} \dot{\theta_2} \sin(\theta_2) + m_2 a_2 r_1 u_1 \cos(\theta_1)
\end{aligned}
$$

$$H_5 = a_3 m_3 \left(h_1 {r_1}^2 \sin(\theta_1 + \theta_2) - r_1 v_1 \sin(\theta_1 + \theta_2) \right) + a_3 m_3 \left(l_2^* {\dot{\theta_1}}^2 \sin(\theta_2) + r_1 u_1 \cos(\theta_1 + \theta_2) \right) + a_3 m_3 \left(l_2^* {r_1}^2 \sin(\theta_2) - 2 l_2^* r_1 \dot{\theta_1} \sin(\theta_2) \right).$$

The entries $Q_{v,i}, i \in \{1, 2, ..., 5\}$, of the column Q_v read

$$\begin{aligned}
Q_{v,1} &= F_{x,2} + F_{x,3} - F_{y,1} \sin(\delta_1) - F_{y,4} \sin(\delta_4 - \theta_1) \\
&\quad - F_{y,5} \sin(\delta_5 - \theta_1) - F_{y,6} \sin(\delta_6 - \theta_1 - \theta_2) \\
&\quad - F_{y,7} \sin(\delta_7 - \theta_1 - \theta_2) - F_{y,8} \sin(\delta_8 - \theta_1 - \theta_2), \\
Q_{v,2} &= F_{y,1} \cos(\delta_1) + F_{y,2} + F_{y,3} + F_{y,4} \cos(\delta_4 - \theta_1) \\
&\quad + F_{y,5} \cos(\delta_5 - \theta_1) + F_{y,6} \cos(\delta_6 - \theta_1 - \theta_2) \\
&\quad + F_{y,7} \cos(\delta_7 - \theta_1 - \theta_2) + F_{y,8} \cos(\delta_8 - \theta_1 - \theta_2), \\
Q_{v,3} &= F_{y,1} (a_1 \cos(\delta_1)) + F_{y,2} (-b_1) + F_{y,3} (-b_2) \\
&\quad + F_{y,4} (-b_3 \cos(\delta_4) - h_1 \cos(\delta_4 - \theta_1)) \\
&\quad + F_{y,5} (-b_4 \cos(\delta_5) - h_1 \cos(\delta_5 - \theta_1)) \\
&\quad + F_{y,6} (-b_5 \cos(\delta_6) - h_1 \cos(\delta_6 - \theta_1 - \theta_2) \\
&\quad - l_2^* \cos(\delta_6 - \theta_2)) \\
&\quad + F_{y,7} (-b_6 \cos(\delta_7) - h_1 \cos(\delta_7 - \theta_1 - \theta_2) \\
&\quad - l_2^* \cos(\delta_7 - \theta_2)) \\
&\quad + F_{y,8} (-b_7 \cos(\delta_8) - h_1 \cos(\delta_8 - \theta_1 - \theta_2) \\
&\quad - l_2^* \cos(\delta_8 - \theta_2)), \\
Q_{v,4} &= F_{y,4} (b_3 \cos(\delta_4)) + F_{y,5} (b_4 \cos(\delta_5)) \\
&\quad + F_{y,6} (b_5 \cos(\delta_6) + l_2^* \cos(\delta_6 - \theta_2)) \\
&\quad + F_{y,7} (b_6 \cos(\delta_7) + l_2^* \cos(\delta_7 - \theta_2)) \\
&\quad + F_{y,8} (b_7 \cos(\delta_8) + l_2^* \cos(\delta_8 - \theta_2)), \\
Q_{v,5} &= F_{y,6} (b_5 \cos(\delta_6)) + F_{y,7} (b_6 \cos(\delta_7)) \\
&\quad + F_{y,8} (b_7 \cos(\delta_8)).
\end{aligned}$$

REFERENCES

[1] Eurostat, "Freight transport statistics," 2014. [Online]. Available: http://ec.europa.eu/eurostat/statistics-explained/index.php

[2] European Commission, *EU Transport in Figures 2012*. Luxembourg City, Luxembourg: Publications office of the European Union, 2012.

[3] B. Kraaijenhagen *et al.*, *Greening and Safety Assurance of Future Modular Road Vehicles: Book of Requirements*, Oct 2014. [Online]. Available: https://www.han.nl/international/english/about-han/news/greening-and-sa fety-assur/_attachments/htas_ems_bookofrequirements_oct2014.pdf

[4] R. A. National Transport Commission, "Performance-based standards scheme—The standards and vehicle assessment rules," 2008. [Online]. Available: https://www.nhvr.gov.au/files/resources/0020-pbsstdsvehassrules.pdf

[5] W. Henri, "Automatic steering device for swiveling bogies," U.S. Patent 1,876,684, Sep. 13, 1932. [Online]. Available: http://www.google.nl/patents/US1876684

[6] J. Wouter, "Bogie vehicle steering mechanism," U.S. Patent 2,083,166, Jun. 8, 1937. [Online]. Available: http://www.google.com/patents/US2083166

[7] P. Bolzern, R. M. DeSantis, and A. Locatelli, "An input-output linearization approach to the control of an n-body articulated vehicle," *J. Dyn. Syst., Meas. Control*, vol. 123, no. 3, pp. 309–316, 2001.

[8] M. M. Michalek, "A highly scalable path-following controller for n-trailers with off-axle hitching," *Control Eng. Prac.*, vol. 29, no. 0, pp. 61–73, 2014. [Online]. Available: http://www.sciencedirect.com/science/article/pii/S0967066114001269

[9] R. Orosco-Guerrero, E. Aranda-Bricaire, and M. Velasco-Villa, "Global path-tracking for a multi-steered general n-trailer," *Proc. 15th IFAC World Congr.*, vol. 15, no. 1, pp. 239–239, 2002.

[10] P. Ritzen, E. Roebroek, N. van de Wouw, H. Nijmeijer, and Z.-P. Jiang, "Trailer steering control for a tractor-trailer robot," *IEEE Trans. Control Syst. Technol.*, vol. 24, no. 4, pp. 1240–1252, Jul. 2016.

[11] M. Sampei, T. Tamura, T. Kobayashi, and N. Shibui, "Arbitrary path tracking control of articulated vehicles using nonlinear control theory," *IEEE Trans. Control Syst. Technol.*, vol. 3, no. 1, pp. 125–131, Mar. 1995.

[12] X. Ding, S. Mikaric, and Y. He, "Design of an active trailer-steering system for multi-trailer articulated heavy vehicles using real-time simulations," *Proc. Inst. Mech. Eng., Part D, J. Automobile Eng.*, vol. 227, no. 5, pp. 643–655, 2013.

[13] M. M. Islam and Y. He, "An optimal preview controller for active trailer steering systems of articulated heavy vehicles," SAE Technical Paper, Warrendale, PA, USA, Tech. Rep. no. 2011-01-0983, 2011.

[14] R. Roebuck, A. Odhams, K. Tagesson, C. Cheng, and D. Cebon, "Implementation of trailer steering control on a multi-unit vehicle at high speeds," *J. Dyn. Syst., Meas. Control*, vol. 136, no. 2, 2014, Art. no. 021 016.

[15] S. T. Oreh, R. Kazemi, and S. Azadi, "A new desired articulation angle for directional control of articulated vehicles," *Proc. Inst. Mech. Eng., Part K, J. Multi-Body Dyn.*, vol. 226, no. 4. , pp. 298–314, Dec 2012.

[16] N. Hata, T. Fujishiro, K. van Bremen-Ito, S. Takahashi, and S. Hasegawa, *A Control Method for 4WS Truck to Suppress Excursion of a Body Rear Overhang*. Warrendale, PA, USA: Soc. Autom. Eng., 1989.

[17] B. A. Jujnovich and D. Cebon, "Path-following steering control for articulated vehicles," *J. Dyn. Syst., Meas., Control*, vol. 135, no. 3, 2013, Art. no. 031006.

[18] B. Jujnovich, C. Odhams, R. L. Roebuck, and D. Cebon, "Implementation of active rear steering of a tractor/semi-trailer," in *Proc. 10th Int. Symp. Heavy Veh. Transport Technol.*, 2008, pp. 358–367.

[19] J. Kandathil Jacob, "Improved command steering for a b-double truck combination," Master's thesis, Eindhoven Univ. Technol., Eindhoven, The Netherlands, Oct 2012, D&C 2012.051. [Online]. Available: http://www.mate.tue.nl/mate/pdfs/12050.pdf

[20] H. B. Pacejka, *Tyre and Vehicle Dynamics*, 2nd ed. London, U.K.: Butterworth-Heinemann, 2006.

[21] P. Hatzidimitris, "Active trailer steering control for longer heavier vehicles," Master's thesis, Eindhoven Univ. Technol., Eindhoven, The Netherlands, 2015, DC 2015.065. [Online]. Available: http://repository.tue.nl/840236

[22] K. Kural, A. Prati, I. Besselink, J. Pauwelussen, and H. Nijmeijer, "Validation of longer and heavier vehicle combination simulation models," *SAE Int. J. Commer. Veh.*, vol. 6, no. 2, pp. 340–352, Sep. 2013.

[23] I. J. M. Besselink, "Vehicle dynamics analysis using simmechanics and tno delft-tyre," IAC 2006 The Mathworks International Automotive Conference, Stuttgart, Germany, Tech. Rep., 2006. [Online]. Available: https://pure.tue.nl/ws/files/3150770/Metis251772.pdf

[24] TASS International, "Delft-tyre," [Online]. Available: https://www.tassinternational.com/delft-tyre

[25] P. Ritzen, "Trailer steering control for an off-axle tractor-trailer robot: reducing the swept path width," Master's thesis, Eindhoven Univ. Technol., Eindhoven, The Netherlands, Jan 2014, D&C 2013.061.

[26] S. Skogestad and I. Postlethwaite, *Multivariable Feedback Control: Analysis and Design.*, Hoboken, NJ, USA: Wiley, 2005.

[27] E. W. Jacobsen, "Multivariable feedback control lecture notes," Stockholm, Sweden: Royal Institute of Technology (KTH), 2007.

Karel Kural received the M.Sc. degree from Czech Technical University, Prague, Czech Republic, in 2008, and is currently working toward the Ph.D. (part-time) degree with the Department of Mechanical Engineering, Eindhoven University of Technology, in the group of Dynamics and Control, Eindhoven, The Netherlands. He is a Researcher at Automotive Research Group, HAN University of Applied Sciences, Nijmegen, The Netherlands. His current research field is vehicle dynamics and control of commercial vehicle combinations, and the driver support systems.

Pavlos Hatzidimitris received the B.Sc. and M.Sc. degrees in mechanical engineering from the Eindhoven University of Technology, Eindhoven, The Netherlands, in 2013 and 2015, respectively. After the graduation, he joined ASML, where he works as a Mechatronics Development Engineer.

Nathan van de Wouw received the M.Sc. (Hons.) and Ph.D. degrees in mechanical engineering from the Eindhoven University of Technology, Eindhoven, The Netherlands, in 1994 and 1999, respectively. He is currently a Full Professor with the Department of Mechanical Engineering, Eindhoven University of Technology. He is also an adjunct Full Professor at the University of Minnesota, Minneapolis, MN, USA, and a (part-time) Full Professor at the Delft University of Technology, Delft, The Netherlands. He has published a large number of journal and conference papers and books. He is currently an Associate Editor for the journals *Automatica* and the IEEE TRANSACTIONS ON CONTROL SYSTEMS TECHNOLOGY. His current research interests are the modeling analysis and control of nonlinear/hybrid systems, with applications to vehicular platooning, high-tech systems, resource exploration, smart energy systems, and networked control systems. In 2015, he received the IEEE Control Systems Technology Award.

Igo Besselink received the M.Sc. degree (with credits) and the Ph.D. degree in mechanical engineering from Delft University of Technology in 1990 and 2000, respectively. He was with Fokker Aircraft, while responsible for the analysis of landing gear design loads and stability. Later, he joined TNO in Delft, The Netherlands, where his focus was on development of tyre simulation software and various projects related to vehicle dynamics. Since 2008, he has been full-time employed by the Eindhoven University of Technology, Eindhoven, The Netherlands. He is an Associate Professor at the Eindhoven University of Technology. His research interests include tyre modeling, dynamics of commercial vehicles, vehicle control, and battery electric vehicles.

Henk Nijmeijer (F'00) is a Full Professor at Eindhoven University of Technology, and chairs the Dynamics and Control Group. He has published a large number of journal and conference papers and several books, and is or was on the Editorial Board of numerous journals. He is an Editor of *Communications in Nonlinear Science and Numerical Simulations*. He was awarded the IEE Heaviside premium in 1990. He was appointed honorary knight of the "golden feedback loop" (NTNU) in 2011. He is an IFAC Council Member since 2011. Per January 2015, he is Scientific Director of the Dutch Institute of Systems and Control (DISC). He received the 2015 IEEE Control Systems Technology Award.